THE JOURNAL OF PHYSICAL CHEMISTRY B

Article

pubs.acs.org/JPCB

# Structure and Raman Spectra in Cryolitic Melts: Simulations with an ab Initio Interaction Potential

Serpil Cikit,[†] Zehra Akdeniz,*[,‡] and Paul A. Madden[¶]

[†]Department of Mathematics, Halic University, Istanbul, Turkey

[‡]Faculty of Science and Letters, Piri Reis University, 34940 Tuzla, Istanbul, Turkey

[¶]Department of Materials, University of Oxford, Parks Road, OX1 3PH, United Kingdom

**ABSTRACT:** The Raman spectra of cryolitic melts have been calculated from molecular dynamics computer simulations using a polarizable ionic potential obtained by force-fitting to ab initio electronic structure calculations. Simulations which made use of this ab initio derived polarizable interaction potential reproduced the structure and dynamical properties of crystalline cryolite, $Na_3AlF_6$, rather well. The transferability of the potential model from solid state to the molten state is tested by comparing results for the Raman spectra of melts of various compositions with those previously obtained with empirically developed potentials and with experimental data. The shapes of the spectra and their evolution with composition in the mixtures conform quite well to those seen experimentally, and we discuss the relationship between the bands seen in the spectra and the vibrational modes of the $AlF_n^{(3-n)}$ coordination complexes which are found in the $NaF/AlF_3$ mixtures. The simulations thus enable a link between the structure of the melt as derived through Raman spectroscopy and through diffraction experiments. We report results for quantities which relate to the degree of cross-linking between these coordination complexes and the diffusive properties of ions.

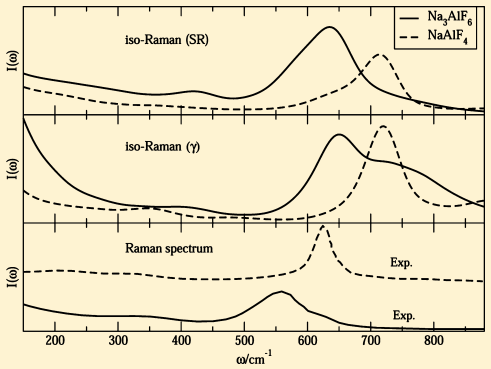


## INTRODUCTION

In recent papers,[1,2] it has been shown how it is possible to simulate the Raman spectra of moderately complex molten salts. The simulations offer a way of bridging an interpretative gap between the structures as seen spectroscopically and that is understood from diffraction experiments. In spectroscopy, attention is focused on the coordination complexes responsible for the discrete Raman bands seen in the spectra of melts with polyvalent cations,[3] which are similar to those seen in a molecular system, whereas in diffraction experiments, the data is discussed from a more atomistic perspective in terms of radial correlations in an ionic mixture.[4,5] A further prospect is to relate the insights into the local structures in the melts, gained from spectroscopy and diffraction, to the transport properties of the melts.[6]

Ionic melts of the general composition $MX_3/AX$ (where M is a trivalent metal, X is a halogen, and A is an alkali) are of interest in several electrochemical technologies.[7,8] Molten cryolite ($Na_3AlF_6$ or $AlF_3/3NaF$) is a stoichiometric compound in a continuous range of liquid $AlF_3/NaF$ solutions (cryolitic melts), which has special interest because of its role in the industrial Hall–Heroult process[7] for the electrodeposition of Al metal from alumina. For this reason, it has been studied extensively. A comprehensive Raman study has been made, by Gilbert and co-workers[9−11] in particular, which has provided the working model for the way that the mixture composition affects the coordination structure.

In discussing the coordination structure of polyvalent cations in alkali halide solutions, it has often been presumed that the cation will have a preferred coordination number for a given anion which is determined, in large part, by the ratio of the cation to anion ionic radii. However, Gilbert and co-workers[9−11] have proposed that, in the melts of $NaAlF_4$, the only significant aluminum-containing species is the tetrahedral $AlF_4^-$ ion. In the $Na_3AlF_6$ melt (cryolite), the Gilbert experiment assigns the five-coordinated $AlF_5^{2-}$ ion to be by far the dominant environment in liquid cryolite $Na_3AlF_6$. Controversies about this assignment[12] have been resolved in recent work.[13] Furthermore, high temperature NMR measurements[14] have given an alternative experimental window on the evolution of the coordination environment with the melt composition. The predominance of $AlF_5^{2-}$ in molten cryolite, proposed by Gilbert is consistent with the NMR data.[14,15]

The coordination number of the polyvalent cations in these mixtures may be significant for other chemical and physical properties. The (Lewis) acid–base properties of the melt, and hence the solvating power for other species, are affected by it.[16] Transport properties are also influenced. Consider, for example, the chiolite composition ($Na_5Al_3F_{14}$): if all the $Al^{3+}$ ions in this melt were six or five coordinate, there would be insufficient fluoride ions in the melt for them to complete their coordinate

**Received:** August 12, 2013
**Revised:** January 7, 2014
**Published:** January 17, 2014

shells without some sharing of anions between cations because 18 $F^-$ ions would be required in the six-coordinate case for the 3 $Al^{3+}$ in the stoichiometric formula and 15 would be required in the five-coordinate case. The cross-linking between the coordinate shells induced by the shared anions can dramatically increase the viscosity of a melt.[17] As the $AlF_3$/NaF mixture becomes more concentrated in $Al^{3+}$ ions, the coordination number drops, according to Gilbert's observation, which means that the degree of cross-linking is reduced compared to what might be expected if the coordination state is constant. The opposite tendency has been noted for polyvalent ions in chloride melts,[2,18] whereas in LiF:$BeF_2$ mixtures, the $Be^{2+}$ coordination number stays constant, and the mixtures become very viscous at high $BeF_2$ concentration.[19] The underlying chemical reasons for this difference in behavior have not yet been identified.

The present work is a further development of a previous simulation study[20] in which a theoretical model for the fluctuating polarizability responsible for the Raman spectrum (see below) was combined with a polarizable ionic interaction potential in a molecular dynamics framework to calculate Raman spectra for melts of various compositions and to compare with experimental spectra. Similar methods had previously been used on chloride melts.[2] Although the calculated spectra (and other physical properties) for the cryolite melts strongly resembled the experimental ones, an analysis of the coordination numbers of the $Al^{3+}$ ions suggested that these were systematically larger than those that had been deduced from the experiments and, in particular, that 5 was not the dominant coordination number for the cryolite composition, whereas both Raman spectroscopy and NMR measurements now show this to be the case. In the previous work, we used an empirical interaction potential which had been parametrized to reproduce structural properties of several $AlF_3$/NaF crystalline compounds,[21] and we further modified it to improve the predicted bands of the vibrational bands as seen in the Raman spectra. We now return to the problem with a polarizable potential derived from first-principles electronic structure calculations[22] according to methods which have now been used to obtain highly realistic potentials for a wide range of ionic materials.[17,19,23] The motivation for revisiting the problem is therefore to further examine the ability of these ab initio generated potentials to predict the properties of complex melts and thereby to validate their use in interpreting the underlying chemical influences on the physical properties across the full range of ionic compounds.

Below, we will use the ab initio fitted polarizable interaction potential[22] to evaluate the structural properties for cryolitic melts and to calculate their Raman spectra. We will also describe the distribution of coordination numbers for the complexes calculated using our simulations. We have calculated Raman spectra across the range of compositions from $NaAlF_4$ to $Na_3AlF_6$ and simultaneously have studied the structure and dynamics of the coordination complexes of the cryolitic melts. Using the methods introduced by Pavlatou et al.,[24] we will link the Raman bands to the normal modes of vibration of the coordination complexes. Comparatively little progress has been made in relating the depolarized Raman spectra of the melts to their microstructure.[3,25] We will show that the depolarized spectra from the simulations with different concentrations are related to vibrations of the coordination complexes in the same manner as the isotropic spectrum.

## RAMAN SPECTRUM DETAILS

A theory of the calculation of the Raman spectrum based on a consideration of the way that the polarizability of a condensed-phase anion is affected by fluctuations in the position of neighboring ions was discussed at length in previous papers,[1,2] and here we simply recall the key points. The general light scattering spectrum expression[3,26,27] of a sample characterized by the scattering vector $\mathbf{q}$ is given below, where the polarizations of the incident and scattered radiation are the Cartesian directions $b$ and $a$. It is proportional to the spectrum of the correlation function of the $\mathbf{q}$ spatial Fourier component of the polarizability density of the system, $\Pi_{ab}$, that is,

$$I_{ab}(\mathbf{q}, \omega) \propto \mathrm{Re} \int_0^\infty dt e^{i\omega t} \langle \Pi_{ab}(\mathbf{q}, t) \Pi_{ab}(\mathbf{q}, 0)^* \rangle \quad (1)$$

For an ionic material, we[29,31] distinguish four contributions to the polarizability

$$\Pi_{ab} = \Pi_{ab}^{\mathrm{SR}} + \Pi_{ab}^{\gamma} + \Pi_{ab}^{B} + \Pi_{ab}^{\mathrm{DID}} \quad (2)$$

The terms $\Pi_{ab}^{B}$ and $\Pi_{ab}^{\gamma}$ represent the changes in the anion polarizability by hyperpolarization via the interionic coulomb field, where $B$ and $\gamma$ are the dipole−quadrupole and dipole−dipole−dipole hyperpolarizabilities of the ion.[28] $\Pi_{ab}^{\mathrm{DID}}$ is the contribution due to first-order dipole-induced dipole effects (DID), and $\Pi_{ab}^{\mathrm{SR}}$ is due to the changes in the polarizability $\alpha_{ab}^{i}$ of an anion by the compression and deformation of the ion by its short-range interactions with its neighbors.[29,30] Detailed expressions for these different polarizability mechanisms in terms of the ionic coordinates are given in earlier papers,[1,29,31] and values for the implicit parameters used in the present simulations are given in ref 22.

The light-scattering spectrum of an ionic system is thus quite complicated as four mechanisms, with different dependencies on the interionic separations, can be expected to contribute. In the calculations, the primary interest is in the isotropic spectrum, which reflects fluctuations in the trace of the polarizability density

$$\Pi_I \equiv \Pi_{xx} + \Pi_{yy} + \Pi_{zz} \quad (3)$$

and which dominates the polarized spectra. It can be shown that only the short-range ($\Pi^{\mathrm{SR}}$) and gamma mechanisms ($\Pi^{\gamma}$) contribute to the trace of $\Pi$ because of the traceless nature of the dipole−dipole interaction tensor and the coulomb field gradient. The isotropic spectrum can thus be regarded as the sum of three terms, the spectra of the autocorrelation functions of $\Pi_I^{\mathrm{SR}}$ and $\Pi_I^{\gamma}$, which we call the SR and $\gamma$ subspectra, as well as the spectrum of their cross-correlation function. As in our previous Raman work,[20] we will also give results for the individual subspectra. These are important as the relevant polarizabilities depend on the interionic coordinates in different ways, and so it might be expected that they would reflect different aspects of the dynamics of the melt. All four mechanisms may contribute to the depolarized spectrum for which we will, again, only discuss the subspectra.

The depolarized subspectra of the melt may be calculated from any one of the five independent anisotropic components of $\boldsymbol{\Pi}$, such as $\Pi_{xy}$. As we discussed in the Raman work,[20] it is possible to calculate reasonably noise free depolarized subspectra for the melts by averaging over the spectrum of $\Pi_{ab}(\mathbf{q} = 0)$ for these five independent components. For the isotropic spectrum, no such averaging is possible, and we have again calculated spectra at the smallest values of $q$ accessible in


dx.doi.org/10.1021/jp4080459 | J. Phys. Chem. B 2014, 118, 1064−1070

the simulation and have exploited the projection method, introduced in ref 1, to get spectra of the quality reported below.

## SIMULATION METHOD

The interaction potential used in the present simulations was obtained by fitting the ab initio information on the forces and dipoles in simulations of pure, crystalline $AlF_3$ and NaF at high temperatures. The transferability of this fit to crystalline cryolite was confirmed by performing further ab initio calculations on cryolite itself and by comparing the forces and multipoles with those predicted by the interaction model;[22] in subsequent MD simulations, the potential reproduced experimental data on phase behavior and ionic conduction[21,22] extremely well. Detailed descriptions of the ab initio force-fitting procedure used to obtain the parameters in a potential chosen from condensed phase, plane-wave density functional, and electronic structure calculations have been given recently[19,23] and will not be repeated here.

The values for all new potential parameters are given in Table 1. The polarization part of the potential includes only the fluoride ion polarization. The values for the ionic polarizability and short-range damping parameters are taken from ref 22. The detailed expressions for this fitted potential are given in the Appendix.

**Table 1. Pair Potential Parameters**[a]

| ion pair | $B_{ij}$ | $\alpha_{ij}$ | $C_{ij}^6$ | $C_{ij}^8$ | $b_{ij}^6$ | $b_{ij}^8$ |
|---|---|---|---|---|---|---|
| $F^-$–$F^-$ | 120.93 | 2.20 | 0.0 | 0.0 | 0.0 | 0.0 |
| $Al^{3+}$–$F^-$ | 111.43 | 2.35 | 0.0 | 0.0 | 0.0 | 0.0 |
| $Na^+$–$F^-$ | 73.79 | 2.10 | 0.0 | 0.0 | 0.0 | 0.0 |
| $Al^{3+}$–$Al^{3+}$ | 93.26 | 2.91 | 0.0 | 0.0 | 1.5 | 0.0 |
| $Na^+$–$Na^+$ | 163.76 | 4.73 | 0.0 | 0.0 | 0.0 | 0.0 |
| $Al^{3+}$–$Na^+$ | 0.0 | 0.0 | 0.0 | 0.0 | 0.0 | 0.0 |

[a]All the parameters are given in atomic units.

The calculations were carried out at temperatures close to the melting point of cryolite. All the runs contained between 500 and 600 ions, depending on stoichiometry. In all cases, the system settled to a density close to the experimental one[32] using a 100 000 step equilibriation run (36 ps) in an NPT ensemble, using the algorithm suggested by Martyna et al.[33]

We then performed a 500 000 step NVT run at the cell volume to which the system had equilibrated at zero external pressure during which time correlation functions and so forth were calculated. Ewald sums were used for all coulomb and multipolar interactions.[34]

## STRUCTURE AND DIFFUSION

In Figure 1, we show a snapshot of the ionic positions taken from the simulation at the chiolite ($Na_5Al_3F_{14}$) composition at 1250 K. $F^-$ ions are shown in red, $Al^{3+}$ ions are shown in blue, and $Na^+$ ions are shown in gray. Lines indicate bonds between Al and F ions if they are separated by less than the first minimum in the radial distribution function. The snapshot indicates that at this composition the melt contains four-, five-, and six-coordinate Al species.

The radial distribution functions (rdf) are given in Figure 2 for three different melt compositions. The Al–F rdf shows a sharp peak followed by a well-defined first minimum. The deep minimum shows that the system is made up of strong $Al^{3+}$-centered coordination complexes with a weak exchange of F ions between species. The Al–Al rdf shows two small prepeaks

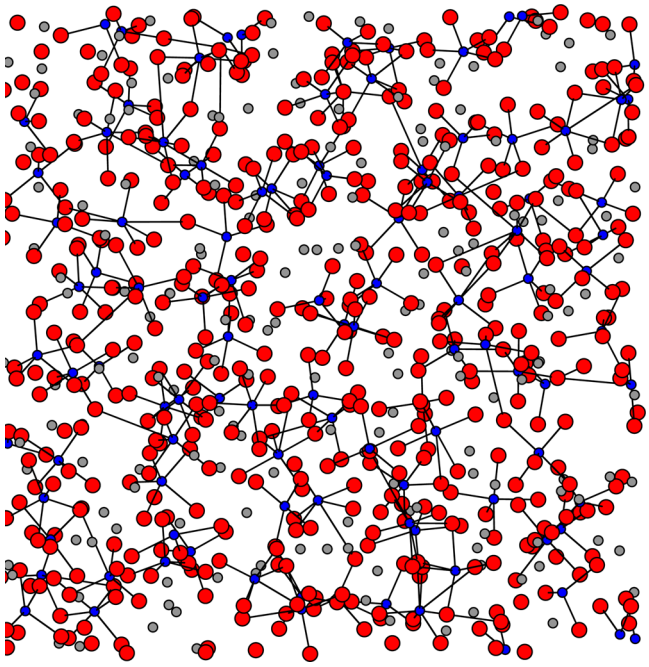

**Figure 1.** Snapshot of the ion positions in simulations of the chiolite composition ($Na_5Al_3F_{14}$). The $F^-$ ions are shown in red, the $Al^{3+}$ in blue, and the $Na^+$ in gray.

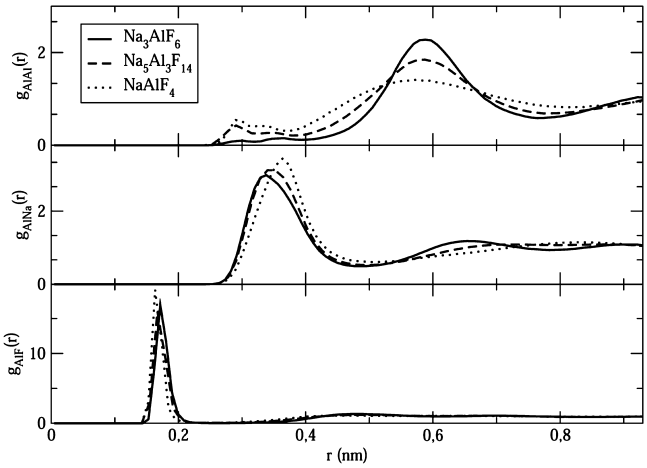


**Figure 2.** The calculated Al–Al (in the top panel), Al–Na (middle), and Al–F (bottom panel) radial distribution functions in $AlF_3$/NaF mixtures are shown for comparison.

which indicates cross-linking between the Al-coordinated species. The two peaks increase in magnitude as we move toward the $NaAlF_4$ composition when the first of the two has a radial position about twice that of the first peak in the Al–F rdf. This is due to $Al^{3+}$ pairs being held together by a bridging $F^-$. The major broad peak, at about 0.6 nm, which is due to correlations between unlinked $Al^{3+}$ coordination complexes, becomes less well-defined as the $AlF_3$ concentration increases. The first peak in the Al–Na distribution is strong and overlaps the position of the prepeaks in the Al–Al rdf . This suggests a competition between the alkali ions and a second five-coordinated $Al^{3+}$ ion bound via a linking $F^-$ ion for the next-neighbor position.

In cryolite, the F–Al calculated partial running coordination number given in the top panel of Figure 3 shows that the coordination number for $F^-$ ions around the $Al^{3+}$ ion is about


dx.doi.org/10.1021/jp4080459 | J. Phys. Chem. B 2014, 118, 1064–1070

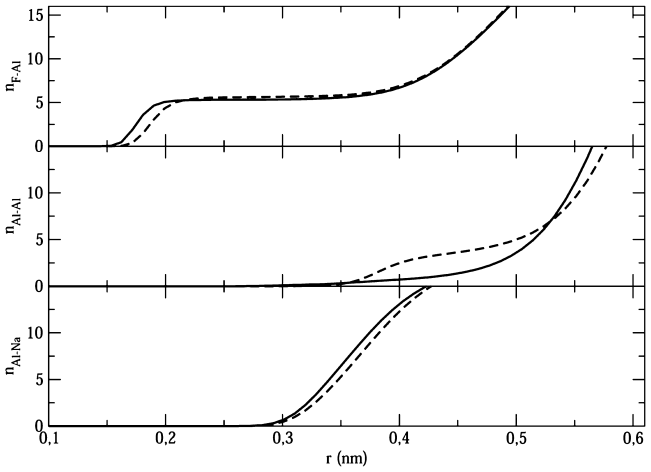


**Figure 3.** The calculated partial running coordination numbers in cryolite for F–Al (in the top panel), Al–Al (middle), and Al–Na (bottom) are compared with the results (shown as dashed lines) obtained using the interaction potential in ref 20.

five. This is consistent with the $AlF_5^{2-}$ units being the predominant species at the cryolite composition. In the mid panel from the Al–Al coordination, it is clear that each Al-centered coordination complex is essentially free in cryolite itself rather than being a part of a fluorine-sharing network, but as the composition shifts toward that of $NaAlF_4$, the increase in size of the prepeak and the increased breadth of the main peak suggest a tendency toward cross-linking. However, if $AlF_5^{2-}$ were the predominant species in $NaAlF_4$, the prepeak would be much stronger than is observed as stoichiometry would demand a much higher degree of cross-linking than at the cryolite composition.

The distribution of coordination numbers is obtained by calculating the probability that an $Al^{3+}$ ion has a given number of neighbors at any instant. Neighbors are defined as ions inside the first shell, which corresponds to the position of the minimum of the rdf illustrated in Figure 2. Table 2 shows the

**Table 2. Distribution of Coordination Numbers in $AlF_3$/NaF[a]**

| | $Al^{3+}$ Coordination numbers | | |
|---|---|---|---|
| $AlF_3$/NaF mixtures | 4 | 5 | 6 |
| $Na_3AlF_6$ | 1.63% (0.8%) | 58.13% (32.53%) | 40.20% (66.64%) |
| $Na_5Al_3F_{14}$ | 27.28% (10.65%) | 60.79% (55.46%) | 11.93% (33.87%) |
| $NaAlF_4$ | 75.28% (34.83%) | 22.24% (48.7%) | 2.47% (16.44%) |

[a]The values in the parentheses are taken from ref 20.

percentage of $Al^{3+}$ ions which are four-, five-, or six-coordinate at the different compositions and at a temperature of 1250 K. The table shows that $AlF_5^{2-}$ ion is the predominant group in both the cryolite $Na_3AlF_6$ and $Na_5Al_3F_{14}$ composition, whereas in $NaAlF_4$, it is $AlF_4^-$. The results given in the table agree with those deduced from the analysis of the experimental spectrum, illustrating that the five-coordinate species is already the majority species in molten cryolite and that $AlF_4^-$ predominates in $NaAlF_4$.[10,11]

This analysis directly confirms a shifting equilibrium between the different coordination structures, which was invoked to explain the concentration dependence of the positions of the isotropic Raman bands and the fluorine chemical shifts observed experimentally.[13−15] In brackets, we show the results from our previous results of Raman work.[20] The discrepancy between the two simulation results must reflect the changes in the interaction potentials used. The potential used in this work reproduces the experimentally measured coordination of ions to a high degree of fidelity. It has a stronger repulsion between the Al and F ions, which has increased the tendency toward lower coordination numbers. As we will see, this has worsened the predictions of the Raman band positions.

Another important physical quantity, given in Figure 4, is the mean square displacement of the two ionic species in $AlF_3$/NaF

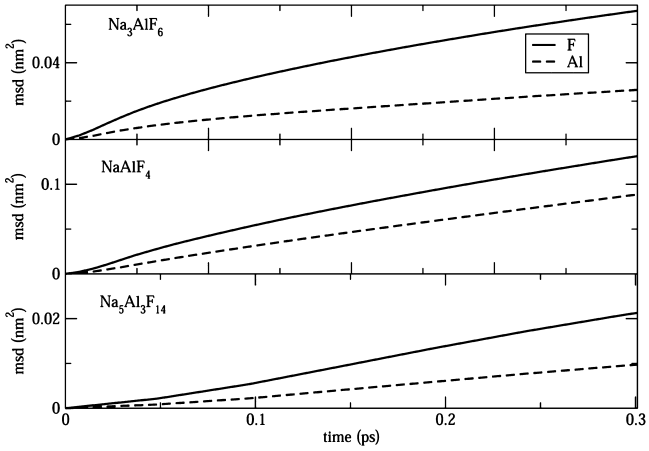


**Figure 4.** Mean square displacements of the ions in the present model for $AlF_3$ and NaF mixtures of various compositions.

mixtures as a function of time at 1250 K. These plots show that the diffusion is fast for all three compositions, and so the system has not become glassy because of cross-linking of coordination shells. In LiF:$BeF_2$ mixtures, by contrast, where the coordination number of the $Be^{2+}$ ions does not change as the melt composition changes, the viscosity rises sharply (and the diffusion coefficient drops) as the mixture becomes concentrated in $BeF_2$ because of the increased degree of cross-linking between the $BeF_4^{2-}$ coordination complexes. On the (short) time scales illustrated, the individual $F^-$ and $Al^{3+}$ ions are linked within their coordination complexes, and the displacement of the $F^-$ ions is larger than that of the $Al^{3+}$ ions because of the rotation of these complexes.

## SIMULATED RAMAN SPECTRA RESULTS

**Isotropic Spectrum.** In this section, we present the Raman spectra calculated from the MD simulations for NaF/$AlF_3$ mixtures at 1250 K. For all mixtures of interest, we show the subspectra associated with the SR and $\gamma$ polarizability mechanisms in the upper panels of Figures 5 and 6, respectively. In the bottom panels of the figures, the density of states (DoS) of the symmetric breathing vibrations of four, five, and six-coordinate complexes obtained using the method introduced by Pavlatou at al.[24] are illustrated. As might be expected, the coordination complex involving the smallest number of ligands ($AlF_4^-$) shows the highest symmetric stretching frequency. The comparison of the top and bottom panels shows that the shift in the positions of the main bands in the calculated spectra from one composition to another is consistent with a shift in the equilibrium between four-, five-, and six-coordinate complexes. The bands appear with different weightings in the SR and $\gamma$ subspectra because of the different


dx.doi.org/10.1021/jp4080459 | J. Phys. Chem. B 2014, 118, 1064−1070

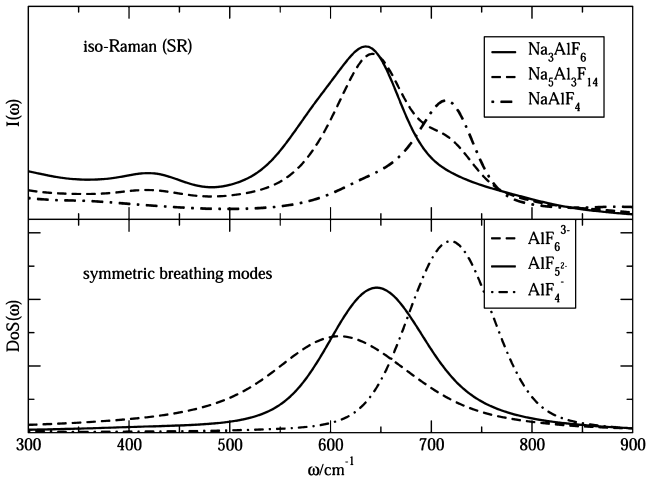


**Figure 5.** Isotropic Raman spectra calculated for the short range (SR, top panel) for three different melt compositions using ab initio derived potential are compared with the density of states (DoS) of the symmetric breathing vibrations of four-, five-, and six-coordinate complexes.

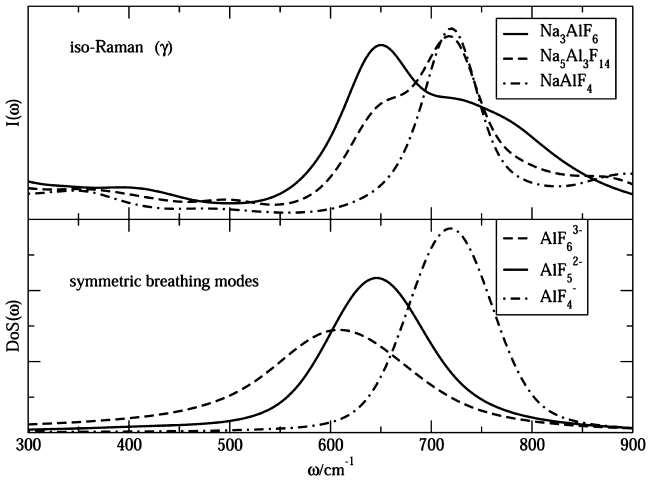


**Figure 6.** Isotropic Raman spectra (in the top panel) calculated for the $\gamma$-hyperpolarizability mechanism at three different melt compositions compared with the DoS spectra of the symmetric breathing vibrations of four-, five-, and six-coordinate complexes.

dependencies of these mechanisms on the interionic separations. In particular, the contribution to the spectra of the vibrations of the four-coordinate units seems to be enhanced in the $\gamma$ spectrum. As we have discussed previously, it is not straightforward to obtain absolute intensities for the different mechanisms from the models for the fluctuating polarizability described above as there is a substantial degree of cancellation between them. We therefore prefer to show the subspectra alone to illustrate the mechanisms by which the vibrational modes affect the fluctuating polarizability and hence cause the observed Raman bands. We do not include the spectral contributions attributed to the cross-correlations between the different mechanisms. These do not introduce new spectral features, but they do shift the relative intensities of the bands.

The relative positions of the bands in the simulated spectra for the $NaAlF_4$ and $Na_3AlF_6$ mixtures are very similar to that seen in the experimental spectra for these systems.[15] Figure 7 demonstrates this similarity: the top two panels show the simulation results for the gamma and SR bands, and the lower

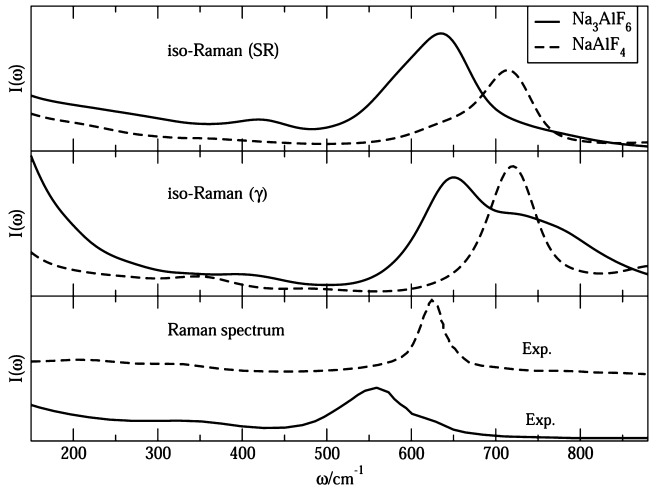


**Figure 7.** The simulated isotropic SR and $\gamma$ subspectra calculated at 1250 K for the cryolite $Na_3AlF_6$ (full line) and $NaAlF_4$ (dashed line) mixtures are shown in the upper two panels, respectively. In the bottom panel, the experimental Raman spectra for $NaAlF_4$ at 1173 K and for $Na_3AlF_6$ at 1293 K are reproduced from ref 15.

panel shows the experimental Raman data. Although the absolute positions of the calculated Raman bands are too high by about 100 cm$^{-1}$, the shift to higher frequencies going from $Na_3AlF_6$ to $NaAlF_4$ is well reproduced. As we have seen in Figures 5 and 6, this shift is due to the lowering of the predominant coordination number. The shapes and widths of both the SR and $\gamma$ subspectra are broadly consistent with the experimental data; the shoulder on the experimental band on the high frequency side in $Na_3AlF_6$ is reproduced in the $\gamma$ subspectrum, though with too high an intensity. An appropriate superposition of the two subspectra would reproduce the experimental bandshapes and their relative positions quite well.

As indicated above and as shown in Table 3, the band positions of the calculated spectra are systematically too high by

**Table 3. Peak Frequencies of the Symmetric Breathing DoS Spectra at 1250 K in $AlF_3$/NaF Mixtures[a]**

| | symmetric breathing modes (cm$^{-1}$) | | |
|---|---|---|---|
| $AlF_3$/NaF mixtures | 6-coord | 5-coord | 4-coord |
| experiment[9] | 510 | 560 | 622 |
| $Na_3AlF_6$ | 594 (544) | 644 (578) | 719 (630) |
| $Na_5Al_3F_{14}$ | 555 (550) | 586 (584) | 719 (631) |
| $NaAlF_4$ | 583 (584) | 600 (598) | 719 (631) |

[a]The values in the parentheses are taken from ref 20.

about 100 cm$^{-1}$ and are poorer than the band positions obtained with our previous simulation potential. This is almost certainly due to the stiffer nature of the short-range repulsion between Al and F ions in the new potential (to which we have, however, attributed the favorable effect on the coordination numbers). Recall that the previous potential was adjusted to improve the predicted vibrational frequencies. The present potential was constructed on a purely ab initio basis without any empirical adjustments. It was, however, parametrized and tested on distorted crystal calculations, where the coordination numbers of the ions are fixed and the relative separations of the ions fluctuate over a very limited range. It could be that the functional form of the potential would be better refined if a


dx.doi.org/10.1021/jp4080459 | J. Phys. Chem. B 2014, 118, 1064−1070

much wider range of distorted coordination environments were included in the set to which the potential model was fitted.

**Anisotropic (Depolarized) Spectrum.** Although the analysis of the coordination structures from the experimental Raman data is based upon the polarized spectrum (to which the isotropic spectrum is the dominant contributor), it is of interest to see how the other modes (other than the symmetric stretches) of the coordination complexes affect the depolarized (anisotropic) spectra. The anisotropic spectrum makes a relatively weak contribution to the (observed) polarized spectrum and introduces several features not attributable to symmetric stretching vibrations. In the top panel of Figure 8,

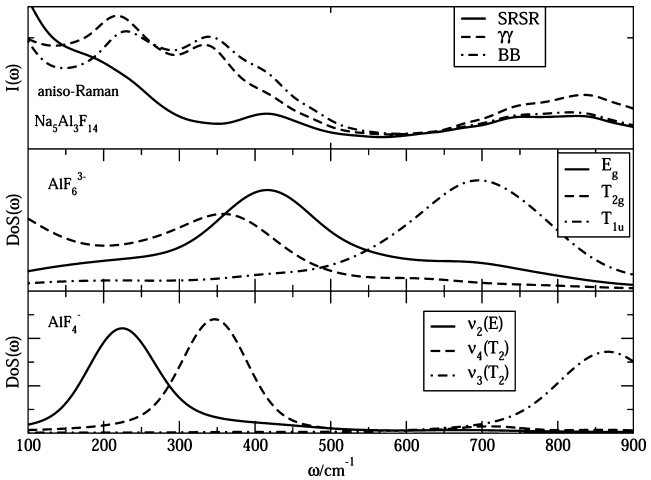


**Figure 8.** Anisotropic subspectra (SR, full line; $\gamma$, dashed line; **B** tensor, dot−dashed line) for the $Na_5Al_3F_{14}$ mixture are shown in the top panel. In the middle panel, the octahedral normal mode vibrational DoS spectra are shown, and in the third panel, the tetrahedral DoS spectra of the $NaAlF_4$ mixture are shown.

we show calculated depolarized spectra for three of the mechanisms which can contribute to the anisotropic polarizability; the remaining DID contribution gives a relatively featureless spectrum. Our ability to compare the band positions with the vibrational modes of the coordination complexes using the Pavlatou method is more limited than for the isotropic case because it is more difficult to identify the vibrational modes of the five-coordinate complex on purely symmetry considerations (other than the symmetric stretch as discussed above). We therefore content ourselves with simply showing the comparison with only the modes of the four- and six-coordinate units. The chiolite composition for the calculated spectrum is chosen because six- and four-coordinated species are both present in significant quantities, which is not true in the other systems studied. The comparison indicates that bands from both species are observed in the calculated spectrum. The $T_{1u}$ mode of the $AlF_6^{3-}$ complex would not be expected to make a strong contribution (it would be Raman-forbidden for an isolated octahedral complex), but the signatures of all the other modes do seem to be present. Of course, without the analysis of the vibrations of the five-coordinate complex, it would not be appropriate to present a definitive assignment.

Overall, it is clear that the effect of the shifting equilibrium between coordination complexes and the way they affect the Raman spectrum have been described well by the new ab initio derived potential.

## DISCUSSION

We have presented theoretical Raman spectra obtained for $AlF_3$/NaF melts by using an ab initio derived polarizable interaction potential and have compared these results with our previous results of empirical polarizable ion interaction potentials. The ab initio derived polarizable interaction potential appears to have reproduced the structural properties of molten $AlF_3$/NaF mixtures well.

The interesting thing about the results, compared to the previous theoretical Raman spectra study[20] on $AlF_3$/NaF mixtures where an empirical potential was used, is that they show the five-coordinate $AlF_5^{2-}$ ions to be the main species in cryolite which is in agreement with experimental evidence. The ionic compositions of other mixtures of $Na_5Al_3F_{14}$ and $NaAlF_4$ agree well with experimental data.

The observation that as the composition of these mixtures shifts toward $AlF_3$ the coordination number of the $Al^{3+}$ ions drops, with the consequence that there is a lower degree of cross-linking between coordination complexes than what would be anticipated if it were constant, is an interesting one. The same simulation methods have been used in previous studies of other molten salt mixtures, including LiF:$BeF_2$ (where the $Be^{2+}$ coordination number remains constant) and LiCl:$LaCl_3$ (where the coordination number increases). The difference in behavior has a consequence for the physical properties of these melts, and here, we have linked the relatively high degree of fluidity across the composition range in NaF:$AlF_3$ compared to LiF:$BeF_2$ to this phenomenon.

Overall, this simulation work described the structure and Raman spectra of molten $AlF_3$/NaF well by using the ab initio derived polarizable interaction. However, there remains a modest difference between the experimental and the calculated vibrational frequencies which results from using potential parameters calculated for the crystalline state as opposed to the experimental data which were taken in the liquid state of cryolite. In future work, we aim to examine the dynamic and vibrational properties and the cation effect on the $AlF_3$/MF mixtures (where the alkali metal M goes from Li to Cs) by using the MD method with a force-fitted potential. This should bring to the work the useful addition of how cation size plays a role in the interpretation of Raman spectra in real liquid systems.

## APPENDIX: INTERACTION POTENTIAL

The interaction potential consists of a pair potential of Born−Mayer form together with an account of interionic polarization.[35] The pair potential, in general, is written

$$V(r_{ij}) = B^{ij}e^{-\alpha^{ij}r_{ij}} - f_{ij}^{6}(r_{ij})\frac{C_{ij}^{6}}{r_{ij}^{6}} - f_{ij}^{8}(r_{ij})\frac{C_{ij}^{8}}{r_{ij}^{8}} \quad (4)$$

where $C_{ij}^6$ and $C_{ij}^8$ are the dispersion coefficients corresponding to the dipole−dipole and dipole−quadrupole dispersive interactions, respectively. This potential, as used in this work, was force-fitted with the dispersion coefficients set to zero as reported in ref 22.

The $f_{ij}^{(n)}$ are dispersion-damping functions given by

$$f_{ij}^{(n)}(r_{ij}) = 1 - e^{-(b_{ij}^{n}r_{ij})}\sum_{k=0}^{n}\frac{(b_{ij}^{n}r_{ij})^{k}}{k!} \quad (5)$$

Values for all parameters are given in Table 1. The polarization parts of the potential include fluoride ion polarization only.[35,36]


dx.doi.org/10.1021/jp4080459 | J. Phys. Chem. B 2014, 118, 1064−1070

We used a fluoride ion polarizability of 6.70 au and applied a damping function

$$g_{ij}(r_{ij}) = 1 - c_{ij}e^{-(b_{ij}r_{ij})}\sum_{k=0}^{4}\frac{(b_{ij}r_{ij})^k}{k!} \quad (6)$$

to the interaction between the anion dipoles and the cation charges with $b_{FAl} = 2.10$, $b_{FNa} = 1.71$, $c_{FAl} = 1.65$, and $c_{FNa} = 1.87$ $au^{-1}$.

## AUTHOR INFORMATION


### Corresponding Author

*E-mail: zehra.akdeniz@pirireis.edu.tr.


### Notes

The authors declare no competing financial interest.

## ACKNOWLEDGMENTS

One of us (Z.A.) thanks Queen's College for hospitality during part of this work and acknowledges support from TUBITAK.

## REFERENCES


(1) Madden, P. A.; Wilson, M.; Hutchinson, F. C. Raman Spectra of Ionic Liquids: Interpretation via Computer Simulation. *J. Chem. Phys.* **2004**, *120*, 6609−6620.

(2) Glover, W. J.; Madden, P. A. Raman Spectra of Ionic Liquids: A Simulation Study of and Its Mixtures with Alkali Chlorides. *J. Chem. Phys.* **2004**, *121*, 7293−7303.

(3) Papatheodorou, G. N.; Yannopoulos, S. N. Light Scattering from Molten Salts: Structure and Dynamics. In *Molten Salts: From Fundamentals to Applications*; Gaune-Escard, M., Ed.; NATO Science Series II; Springer: Dordrecht, Netherlands, 2002; Vol. *52*, pp 47−106.

(4) Tosi, M. P.; Price, D. L.; Saboungi, M. L. Ordering in Metal Halide Melts. *Annu. Rev. Phys. Chem.* **1993**, *44*, 173−211.

(5) Rovere, M.; Tosi, M. P. Structure and Dynamics of Molten Salts. *Rep. Prog. Phys.* **1986**, *4*, 1001−1081.

(6) Brookes, R.; Davies, A.; Ketwaroo, G.; Madden, P. A. Diffusion Coefficients in Ionic Liquids: Relationship to the Viscosity. *J. Phys. Chem. B* **2005**, *109*, 6485−6490.

(7) Grjotheim, K.; Krohn, C.; Malinovsky, M.; Matiasovsky, K.; Thonstad, J. *Aluminium Electrolysis: Fundamentals of the Hall-Heoult Process*, 2nd ed.; Aluminium-Verlag: Dusseldorf, Germany, 1982.

(8) Matsuura, H.; Takagi, R.; Zbalocka-Malicka, M.; Rycerz, L.; Szczepaniak, W. High Enrichment of Uranium and Rare Earth Elements in Ionic Salt Bath by Countercurrent Electromigration. *J. Nucl. Sci. Technol.* **1997**, *33*, 895−897.

(9) Gilbert, B.; Robert, E.; Tixhon, E.; Olsen, J.; Ostvold, T. Structure and Thermodynamics of NaF-$AlF_3$ Melts with Addition of $CaF_2$ and $MgF_2$. *Inorg. Chem.* **1996**, *35*, 4198−4210.

(10) Robert, E.; Olsen, J.; Danek, V.; Tixhon, E.; Ostvold, T.; Gilbert, B. Structure and Thermodynamics of Alkali Fluoride−Aluminum Fluoride−Alumina Melts. Vapor Pressure, Solubility and Raman Spectroscopic Studies. *J. Phys. Chem. B* **1997**, *101*, 9447−9457.

(11) Gilbert, B.; Materne, T. Reinvestigation of Molten Fluoroaluminate Raman Spectra: The Question of the Existence of $AlF_5^{2-}$ Ions. *Appl. Spectrosc.* **1990**, *44* (2), 299−305.

(12) Brooker, M. H.; Berg, R. W.; Von Barner, J. H.; Bjerrum, N. J. Raman Study of the Hexafluoroaluminate Ion in Solid and Molten FLINAK. *Inorg. Chem.* **2000**, *39*, 3682−3689.

(13) Auguste, F.; Tkatcheva, O.; Mediaas, H.; Ostvold, T.; Gilbert, B. The Dissociation of Fluoroaluminates in FLINAK and CsF-KF Molten Mixtures: A Raman Spectroscopic and Solubility Study. *Inorg. Chem.* **2003**, *42*, 6338−6344.

(14) Lacassagne, V.; Bessada, C.; Florian, P.; Bouvet, S.; Ollivier, B.; Coutures, J. P.; Massiot, D. Structure of High Temprature NaF-$AlF_3$-$AlO_3$ Melts: A Multinuclear NMR Study. *J. Phys. Chem. B* **2002**, *106*, 1862−1868.

(15) Robert, E.; Lacassagne, V.; Bessada, C.; Massiot, D.; Gilbert, B.; Coutures, J.-P. Study of NaF-$AlF_3$ Melts by High Temperature $^{27}Al$ NMR Spectroscopy: Comparision with Results from Raman Spectroscopy. *Inorg. Chem.* **1999**, *38*, 214−217.

(16) Duffy, J. A.; Ingram, M. D. Establishment of an Optical Scale for Lewis Basicity in Organic Oxyacids, Molten Salts and Glasses. *J. Am. Chem. Soc.* **1971**, *93*, 6448−6454.

(17) Heaton, R. J.; Madden, P. A. Fluctuating Ionic Polarizabilities in the Condensed Phase: First-Principles Calculations of the Raman Spectra of Ionic Melts. *Mol. Phys.* **2008**, *106*, 1703−1719.

(18) Okamoto, T.; Suziki, S.; Shiwaku, H.; Ikeda-Ohno, A.; Yaita, T.; Madden, P. A. Local Coordination about $La^{3+}$ in Molten $LaCl_3$ and Its Mixtures with Alkali Chlorides. *J. Phys. Chem. A* **2010**, *114*, 4664−4671.

(19) Salanne, M.; Simon, C.; Turq, P.; Heaton, R. J.; Madden, P. A. A First-Principles Description of Liquid $BeF_2$ and Its Mixtures with LiF: Network Formation in LiF-$BeF_2$. *J. Phys. Chem. B* **2006**, *110*, 11461−11467.

(20) Akdeniz, Z.; Madden, P. A. Raman Spectra of Ionic Liquids: A Simulation Study of $AlF_3$ and Its Mixtures with NaF. *J. Phys. Chem. B* **2006**, *110*, 6683−6691.

(21) Foy, L.; Madden, P. A. Ionic Motion in Crystalline Cryolite. *J. Phys. Chem. B* **2006**, *110*, 15302−15311.

(22) Foy, L. Ph.D. Thesis, University of Edinburgh, 2009.

(23) Heaton, R. J.; Brookes, R.; Madden, P. A.; Salanne, M.; Simon, C.; Turq, P. A First-Principles Description of Liquid $BeF_2$ and Its Mixtures with LiF: Potential Development and $BeF_2$. *J. Phys. Chem. B* **2006**, *110*, 11454−11460.

(24) Pavlatou, E. A.; Madden, P. A.; Wilson, M. The Interpretation of Vibrational Spectra of Ionic Melts. *J. Chem. Phys.* **1997**, *107*, 10446−10457.

(25) Photiadis, G. M.; Borresen, B.; Papatheodorou, G. N. Vibrational Modes and Structures of Lanthanide Halide-Alkali Halide Binary Melts $LnBr_3$-KBr (Ln=La, Nd, Gd) and $NdCl_3$-ACl (A=Li, Na, K, Cs). *J. Chem. Soc., Faraday Trans.* **1997**, *94*, 2605−2613.

(26) Berne, B. J.; Pecora, R. *Dynamic Light Scattering*; John Wiley: New York, 1976.

(27) Madden, P. A. Liquids, Freezing and the Glass Transition. *Les Houches Session LI*; Hansen, J.-P. et al., Eds.; North Holland: Amsterdam, 1991; pp 547−627.

(28) Buckingham, A. D. Permanent and Induced Molecular Moments and Long-Range Intermolecular Forces. *Adv. Chem. Phys.* **1967**, *12*, 107−142.

(29) Madden, P. A.; Board, J. Light Scattering By Liquid and Solid Sodium Chloride. A Simulation Study. *J. Chem. Soc., Faraday Trans. 2* **1987**, *83*, 1891−1908.

(30) Fowler, P. W.; Madden, P. A. Fluctuating Dipoles and Polarizabilities in Ionic Materials: Calculations on LiF. *Phys. Rev. B* **1985**, *31*, 5443−5455.

(31) Madden, P. A.; Board, J.; O'Sullivan, K.; Fowler, P. W. Light Scattering by Alkali Halide Melts: A Computer Simulation Study. *J. Chem. Phys.* **1991**, *94*, 918−927.

(32) Ostvold, T.; Fernandez, R. Surface Tension and Density of Molten Fluorides and Fluoride Mixtures Containing Cryolite. *Acta Chem. Scand.* **1989**, *43*, 151−159.

(33) Martyna, G. J.; Tobias, D. J.; Klein, M. L. Constant Pressure Molecular Dynamics Algorithms. *J. Chem. Phys.* **1994**, *101* (5), 4177−4189.

(34) Aguado, A.; Madden, P. A. Ewald Summation of Electrostatic Multipole Interactions up to the Quadrupolar Level. *J. Chem. Phys.* **2003**, *119*, 7471−7483.

(35) Madden, P. A.; Wilson, M. Covalent Effects in Ionic Systems. *Chem. Soc. Rev.* **1996**, *25*, 339−350.

(36) Hutchinson, F.; Wilson, M.; Madden, P. A. A Unified Description of $MCl_3$ Systems with a Polarizable Ion Simulation Model. *Mol. Phys.* **2001**, *99*, 811−824.